J Mater Sci: Mater Electron (2021) 32:7765–7777

Preparation of MoS_2-reduced graphene oxide/Au nanohybrid for electrochemical sensing of hydrazine

Mahsa Gharani[1,*], Ali Bahari[1], and Shahram Ghasemi[2]

[1] Department of Physics, Faculty of Basic Sciences, University of Mazandaran, Babolsar, Iran
[2] Faculty of Chemistry, University of Mazandaran, Babolsar, Iran

Received: 15 October 2020
Accepted: 6 February 2021
Published online: 22 February 2021

© The Author(s), under exclusive licence to Springer Science+Business Media, LLC part of Springer Nature 2021

ABSTRACT

In the present study, MoS_2/reduced graphene oxide (rGO)/Au (MSRG/Au) nanohybrid was synthesized through one-step hydrothermal method and was applied to fabricate the modified electrode in order to detect hydrazine (N_2H_4, HY). Structure of MSRG/Au nanohybrid was characterized by various analyses including field emission scanning electron microscopy (FESEM), energy dispersive X-ray (EDX), transmission electron microscopy (TEM), and X-ray powder diffraction (XRD). Electrochemical behaviors of MoS_2, MSRG, and MSRG/Au in buffer solution were investigated to show the role of simultaneous presence of rGO carbonaceous material and Au noble metal in improving activities of MoS_2. Amperometric response of MSRG/Au-modified glassy carbon electrode (GC electrode) for oxidation of HY had two linear ranges of 2–30 μM and 30 μM–1.5 mM. Limit of detection (LOD) was estimated as 0.5 μM for HY. Because of the synergistic effect of gold nanoparticles, MSRG/Au nanohybrid had higher electrocatalytic activity, yet with less overpotential for oxidation of HY compared to MoS_2/GC electrode and MSRG/GC electrode. After investigating the effect of intrusive ions on determination of analyte, the sensor maintained its great stability, reproducibility, and selectivity for detection of HY. Based on the results, modification of MSRG with Au may be an effective sensing platform to detect HY.

1 Introduction

Detection of hydrazine (N_2H_4, HY), one of critical pollutants in drinking water [1–3] has always been considered as an important matter. HY is commonly used in rocket fuel, tobacco products, reactions of organic matter and pharmaceuticals, as well as coloring tissue, and photography [4–6]. HY can be absorbed through skin, lungs, and gastrointestinal tract and rapidly spreading throughout the body. The use of this substance has been drastically limited over the past two decades due to its detrimental effects on humans' body and the environment, and therefore extensive efforts are being made to replace it with non-toxic alternatives [7–11].

Address correspondence to E-mail: m.a.h.gharani@gmail.com

https://doi.org/10.1007/s10854-021-05496-3

Detection of HY in biological and environmental systems with high sensitivity is of great practical importance [12–14]. There are various methods for precise detection of HY including spectrophotometry, titrimetry, chromatography, and chemiluminescence, most of which are unfortunately time-consuming. Hence, there is a great need for development of an economical and suitable platform for sensitive detection of HY [13]. However, electrochemical methods are straightforward, fast, efficient in terms of sensitivity and selectivity, and low cost. HY is electrochemically active on surface of common electrodes such as graphite screen-printed, and GC electrode [15–17]. Nevertheless, employing these electrodes in the unmodified states poses problems like overpotential or surface saturation. The modified electrodes use carbon nanomaterials, metal nanoparticles, and metal sulfides to improve their [18–26]. Oxidation process of HY is an irreversible process showing only one oxidation peak in cyclic voltammetry (CV).

Various materials have been prepared for the modification of electrode to detect HY analyte. For example, Shahid et al. [6] fabricated a sensor by modifying the electrode with CoO–Au–rGO nanocomposite. The nanocomposites displayed the elevated sensitivity by even 50 times the concentration of intrusive trials in HY. Venkatesh et al. [8] prepared a gold microelectrode-based sensor for detection of HY. Gold nanoporous electrochemical sensor showed high stability and sensitivity toward HY oxidation. Liu et al. [27] fabricated Au–Fe_3O_4–GO nanocomposites for detection of HY with good sensitivity. Limit of detection (LOD) of the samples was evaluated by an amperometric test. Linear detection range was estimated to be between 3.8 μM and 1.4 mM, with a correlation coefficient (R^2) of 0.9991.

According to the previous investigations, molybdenum disulfide (MoS_2) has received a great deal of attention thanks to its unique three-layer structure. Crystalline structure of MoS_2 consists of layers composing of molybdenum bonds and two sulfides [19, 28–31]. The relationship between Mo–S is a strong covalent bond and the sheets are weakly interconnected. Two-dimensional nanomaterials such as graphene and MoS_2 have emerged in materials science owing to their unparalleled physical, chemical, and mechanical properties. Significant progress has also been made in the manufacturing of electrochemical sensors for identification and measurement of a range of chemical and biological molecules using these two-dimensional nanomaterials [32]. MoS_2 nanocomposite-based sensors with reduced graphene oxide (rGO) are more efficient than the ones prepared from pure MoS_2 because of their high active surface area and electron transferability [33–39]. In addition, noble metals such as Au are potent modifiers for increasing electron transfer ability [40–46]. The presence of Au nanoparticles in MoS_2/rGO nanohybrid (MSRG/Au) can enhance its applicability and performance in sensing applications.

Herein, MSRG/Au nanohybrid was synthesized through hydrothermal method and a modified MSRG/Au/GC was fabricated as an efficient sensor for electrochemical detection of HY. Au nanoparticles play an active role in facilitating transfer of electrons, thus the synergistic effect of Au and MSRG improves electrochemical behavior of the sensor for oxidation of HY. In this study a simple, sensitive, and cost-effective sensor is presented with significant electrocatalytic activity for the detection of HY, having tremendous potential for commercial applications. To the best of our knowledge, there is no report on MSRG/Au as electrocatalyst for detection of HY.

2 Experimental procedure

2.1 Apparatus

XRD analyses were carried out by Philips PW1730 device using CuK_α radiation (30 mA, 40 kV) at λ = 1.540598 Å in the 2θ range of 0°–80°. The FESEM device is tuned to the TESCAN model with an accelerator voltage of 15 keV, equipped with energy dispersive X-ray spectroscopy (EDX). TEM analysis was performed using a Philips EM208 instrument at 100 keV. FTIR analysis was performed on a Bruker-Vector 22 between 450 and 4000 cm^{-1} using KBr pellet. Electrochemical behavior of the electrodes was induced using an AUTO LAB 302 N device and a three-electrode system, including GC electrode as working electrode, Ag|AgCl (saturated KCl) as reference electrode, and platinum wire as a counter electrode.

2.2 Synthesis of graphene oxide (GO)

GO was reportedly synthesized with minor modifications [43]. A certain amount of graphite powder

was added to H_2SO_4 and, after placing container in the ice bath, 15 g of $KMnO_4$ was added. Then, H_2O and H_2O_2 were slowly added to the solution and product was washed several times to obtain brownish GO sheets.

2.3 Synthesis of MoS_2 nanosheets

MoS_2 nanosheets were reportedly synthesized with slight modifications through hydrothermal method. For this purpose, 0.3 g of $Na_2MoO_4{\cdot}2H_2O$ was added to a certain amount of distilled water, and then 0.1 M HCl was added to the solution to reach pH level of 6.5. After that, 0.8 g of L-cysteine was added to the solution and volume of the solution reached to 80 mL using distilled water. After 2 h, the solution was transferred into a 100-mL Teflon-lined stainless-steel autoclave and heated up to 220 °C for 15 h in the oven. Resulting suspension was washed several times, and then was dried at 60 °C until black powder MoS_2 nanosheets were obtained.

2.4 Synthesis of MSRG nanosheets

MSRG nanosheets were synthesized using hydrothermal method [31]. For this purpose, 0.1 g of the prepared GO was added to MoS_2 suspension (40 mL) under ultrasonication for about 0.5 h. After that, the mixture was transferred into a 100-mL Teflon-lined stainless-steel autoclave and was heated at 220 °C for 15 h. Resulting suspension was washed and centrifuged with water several times, and then was dried at 60 °C for 20 h.

2.5 Synthesis of MoS_2–rGO/Au nanohybrid

Gold nanoparticles (AuNPs) were synthesized according to the previous reports with slight modifications [28, 43]. After boiling $HAuCl_4$ solution (0.01%), 2.5 mL of trisodium citrate solution (1%) was added rapidly. Color of the mixture was slowly changed from brown to wine red, denoting to the formation of AuNPs. After cooling down the mixture to room temperature, AuNPs solution was collected and stored in brown glass bottles at 4 °C. Then, 40 mL of AuNPs was added to $Na_2MoO_4{\cdot}2H_2O$—L-cysteine—GO solution (30 mL) and the mixture was vigorously stirred for 2 h to complete the reaction. After that, the mixture was transferred into a 100-mL Teflon-lined stainless-steel autoclave and was heated at 220 °C for 15 h. Resulting suspension was centrifuged and rinsed with distilled water several times, and then was dried in the oven at 60 °C for 20 h.

2.6 Electrode modification

Before modification, surface of GC electrode (2 mm in diameter) was polished until achieving a mirror-like state by 0.05 μM alumina powder using a polishing cloth. Then, it was washed with distilled water several times. The electrode was cycled in the range of − 1 to 1 V at a scan rate of 50 mV s^{-1} in 0.5 mM H_2SO_4 solution. For fabricating MSRG–Au/GC electrode, 3 mg of MSRG–Au was dispersed in 500 μL of distilled water, and then 5 μL of colloid solution was poured on GC electrode and was dried at ambient temperature. The other modified electrodes were prepared in the same way using MoS_2 and MSRG nanohybrid dispersions.

2.7 Investigation of electrochemical behavior

Electrochemical behaviors of the electrodes were investigated in phosphate-buffered saline (PBS) (0.1 M, pH = 7.4) at room temperature. Voltammetry tests were performed in the range of − 0.2 to 0.6 V at 50 mV s^{-1}. Amperometric response of the MSRG/Au/GC electrode to HY was recorded to estimate (LOD) by successive injections of analyte into stirring the solution of PBS at a constant potential.

3 Results and discussion

3.1 Characterization of MSRG/Au nanohybrid

FESEM images were used to evaluate morphology and size of the nanostructure. Figure S1a–d for GO, Fig. S2a–d for MoS_2, and Fig. S3a–d for MSRG are provided in four different scales in supplemented information. Figure S1a–d shows that GO nanosheets are layered on top of each other with an average thickness of about 24 nm. Figure S2a–d shows MoS_2 nanosheets with an average thickness of about 35 nm. Figure S3a–d illustrates that MSRG nanosheets have less porosity compared to tightly coupled layers of pure MoS_2 nanosheets, with an average thickness of

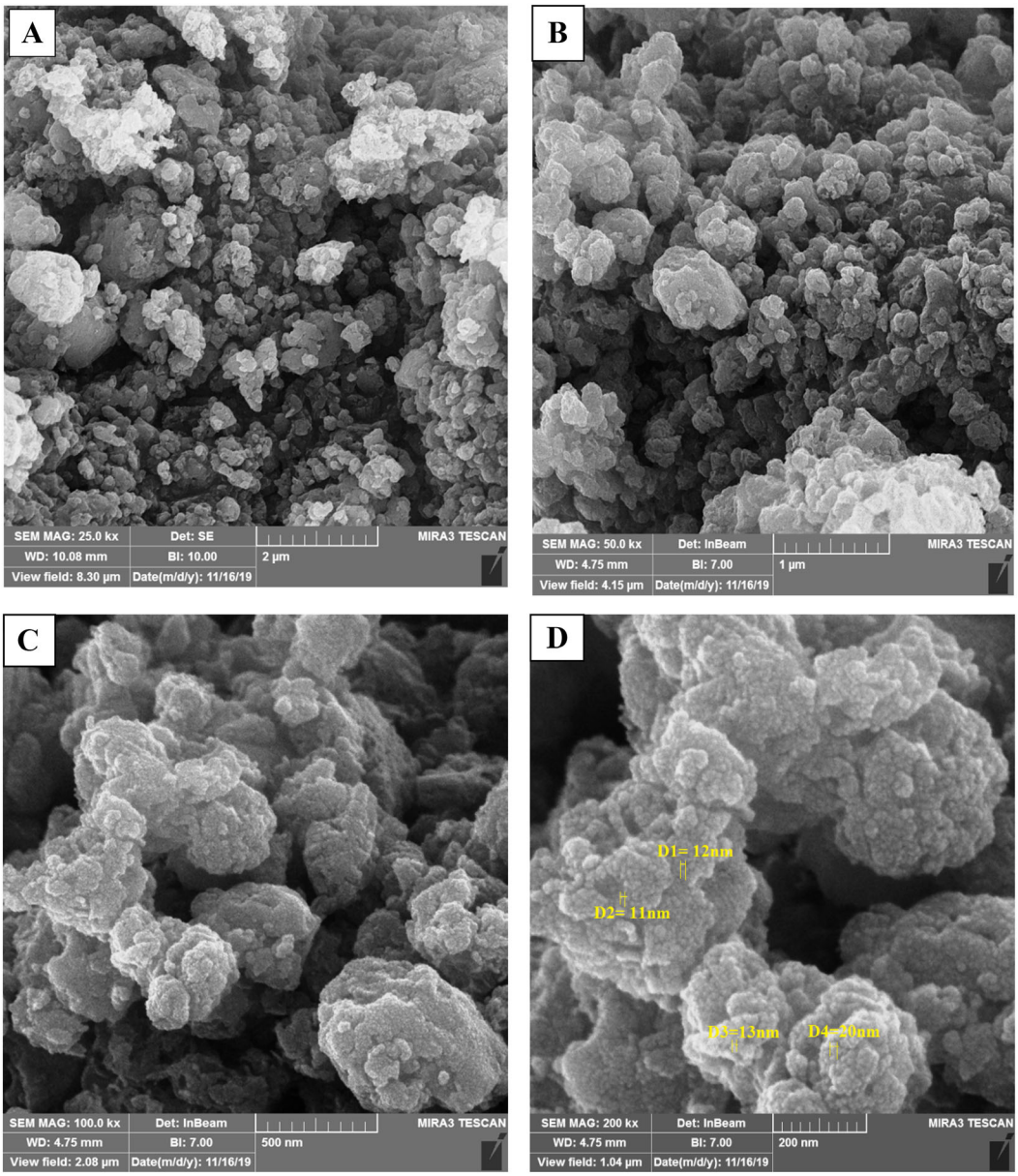

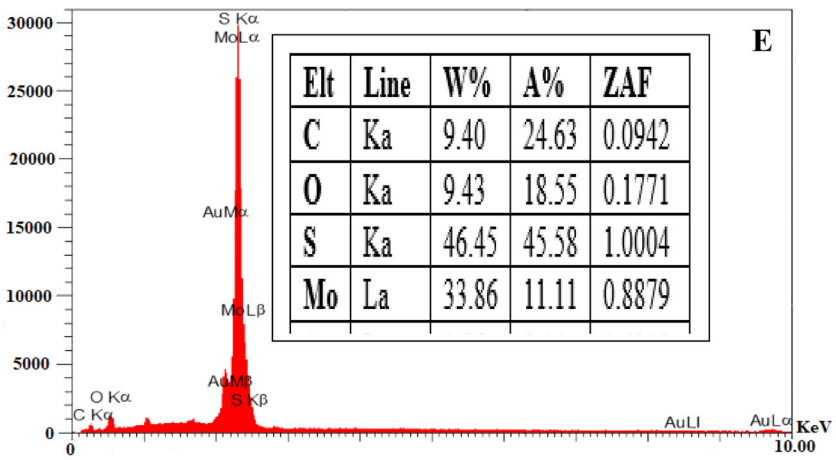

Elt	Line	W%	A%	ZAF
C	Ka	9.40	24.63	0.0942
O	Ka	9.43	18.55	0.1771
S	Ka	46.45	45.58	1.0004
Mo	La	33.86	11.11	0.8879

◀**Fig. 1** FESEM images of **a** MSRG/Au (scale bar 2 μm), **b** MSRG/Au (scale bar 1 μm), **c** MSRG/Au (scale bar 500 nm), **d** MSRG/Au (scale bar 200 nm), and **e** EDX spectra of MSRGG/Au

about 19 nm. Figure 1a–d shows FESEM image at four different scales. AuNPs penetrate almost uniformly into MSRG nanocrystals, reducing porosity and accumulation of MSRG nanocrystals. Average thickness of MSRG/Au was about 14 nm.

Figure 1e shows EDX spectrum of MSRG/Au. The sample contained elements of Mo, S, C, and Au. Proportion of Mo and S elements in nanohybrid was higher than Au element as expected from synthesis process.

Figure 2a, b shows TEM images of the MSRG/Au nanohybrid at two different magnifications. Both GO and MoS_2 had a layered structure; however, MoS_2 had elements with higher atomic mass than GO and appeared as darker nanosheets in images. AuNPs with high atomic mass are formed on nanosheets and appear in dark area of the image due to their properties.

Crystalline structure of MoS_2, MSRG, and MSRG/Au samples was characterized by XRD. For all three samples, diffraction peaks were observed at 2θ of about 18, 33, and 58.6 °C resulting from crystalline phases of MoS_2, corresponding to crystal planes of (013), (100), and (110) of hexagonal structure of MoS_2 (joint committee on powder diffraction standards (JCPDS) 01-081-203) (Fig. 3a). The diffraction peaks appeared at 2θ of 38.16, 44.46, 64.8, and 77.6 °C, and correspond consistently to planes of (111), (200), (220), and (311), respectively, attributing to the cubic structure of Au (JCPDS 00–004-078). The presence of different characteristic peaks in diffraction pattern of sample indicates successful synthesis of MSRG/Au nanohybrid.

Figure 3b represents FTIR spectra of the GO, MSRG nanosheets, and MSRG/Au nanohybrid in the range of 500–4000 cm^{-1}. In the spectrum of GO, the peaks at 3400, 1704, 1618, and 1023 cm^{-1} correspond to O–H hydroxyl group, C=O carbonyl stretching vibrations, C=C non-oxidized graphite structure, and C–O alkoxy stretching vibrations, respectively, indicating GO formation and confirming its presence in nanohybrid.

3.2 Electrochemical studies

Electrochemical behavior of the electrodes modified with nanohybrid for oxidation of HY was investigated through CV method. Figure 4b shows CV of the MSRG/Au/GC electrode in the absence of HY. As can be seen, there is no particular peak in CV of the nanohybrid. Figure 4a shows CV of GC, MoS_2–GC, MSRG–GC, and MSRG–Au–GC electrodes in the

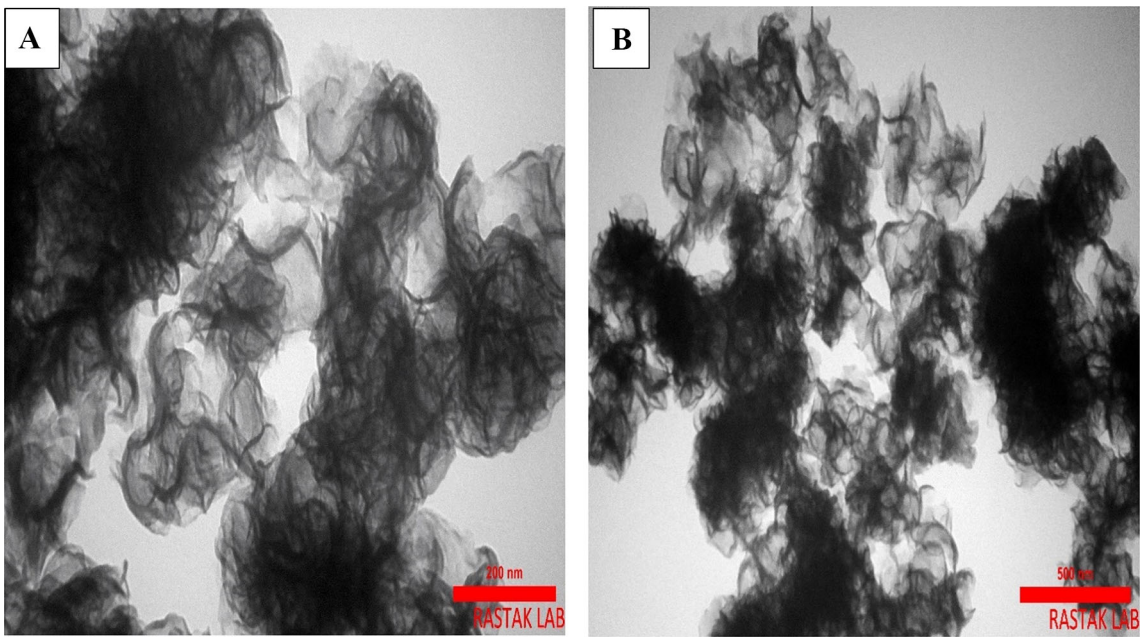

Fig. 2 **a** TEM image MSRG/Au (scale bar 200 nm) and **b** TEM image MSRG/Au (scale bar 500 nm)

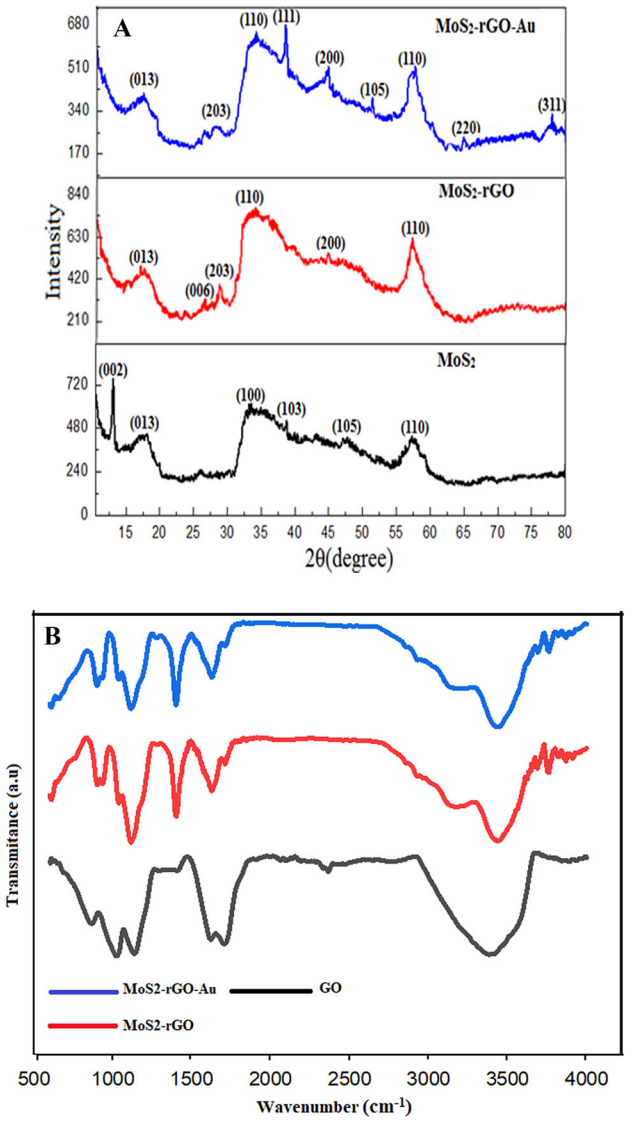

Fig. 3 XRD pattern of **a** MSRG/Au and **b** FTIR spectra of GO, MSRG, and MSRG/Au

presence of 5 mM HY at a scan rate of 50 mV s^{-1}. The MSRG/GC electrode exhibits an oxidation peak at a potential of 0.25 V with current density of 46 µA, whereas the MSRG/Au/GC electrode reveals a sharp oxidation peak at potential of 0.21 V by increasing current density up to 57 µA. On the contrary, the MSRG/Au/GC electrode has a lower overvoltage for oxidation of HY compared to the MSRG nanohybrid, implying that AuNPs can improve catalytic activity of the electrode. In addition, voltammograms were recorded by increasing HY concentration from 1 to 10 mM at 50 mV s^{-1}. Oxidation currents were increased by increasing concentration of HY up to 10 mM.

For evaluating kinetic limitations in process, behavior of the MSRG/Au/GC electrode was investigated in 0.1 M PBS (pH = 7.4) solution containing 5 mM HY by applying different scanning rates from 10 to 300 mV s^{-1} (Fig. 5a). As can be seen in Fig. 5b, anodic peak potential values shift to positive potentials as scanning rate is increased. This shift indicates that oxidation process of HY is kinematically limited. Anodic peak current (*Ip*) is increased by the square root of scanning rate, meaning that process is under diffusion control. As can be seen in (Fig. 5c), there is a linear relationship between peak potential and logarithm of scan rate indicating that oxidation of HY is an entirely irreversible process at GC electrode. Tafel equation is usually applied to obtain information about rate-determining step as follows [17]:

$$Ep = [2.3\,RT/(1-\alpha)\,n_{\alpha}F]\log v + K, \quad (1)$$

where α is the electron transfer coefficient, $n\alpha$ is the number of electrons in rate-determining step, R = 8.314 J K^{-1} mol^{-1}, T = 298, F = 96,485 C mol^{-1}, and K is the constant. Slope value was found to be 110 mV, corresponding to theoretical value of 120 mV. As a result, the proposed mechanism for oxidation of HY at the MSRG/Au/GC electrode may be expressed as follows [47, 48]:

$$N_2H_4 + H_2O \rightarrow N_2H_3 + e^- + H_3O^+ \quad \text{(rate - limiting step)} \quad (2)$$

$$N_2H_3 + 3H_2O \rightarrow N_2 + 3e^- + 3H_3O^+ \quad \text{(fast reaction)} \quad (3)$$

$$N_2H_4 + 4H_2O \rightarrow N_2 + 4H_3O^+ + 4e^- \quad \text{(overall reaction)} \quad (4)$$

CV was used to investigate behavior of the MSRG–Au nanohybrid in 0.1 M KCl solution containing 1 mM $K_3[Fe(CN)_6]/K_4[Fe(CN)_6]$ at a scan rate of 10–400 mVs^{-1}. As shown in Fig. 5d, e, voltammograms exhibit oxidative descending peaks. The amount of I_P is increased by the square root of

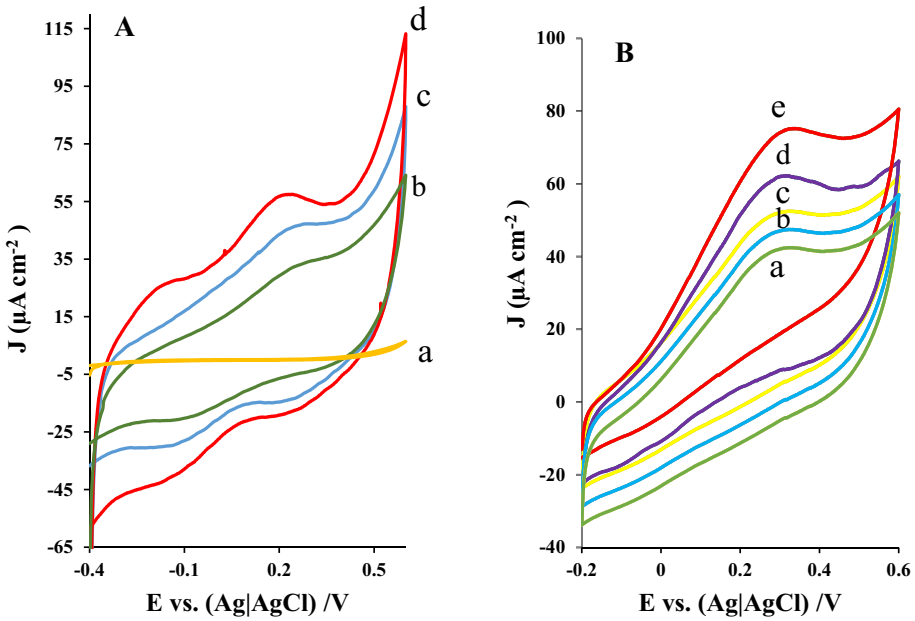

Fig. 4 CVs of **a** bare GC electrode (*a*), MoS_2/GC electrode (*b*), MSRG/GC electrode (*c*), MSRG/Au/GC electrode (*d*) in the presence of 5 mM hydrazine, **b** CVs of MSRG/Au /GC electrode in different concentrations of hydrazine *a* 1, *b* 3, *c* 5, *d* 8, and *e* 10 mM

scanning rate linearly, indicating that oxidation of HY at the MSRG/Au/GC electrode is a diffusion-controlled process.

Amperometric response of the MSRG/Au/GC electrode was measured three times to estimate LOD of HY oxidation. Amperometric response was recorded through successive injections of HY into stirring PBS solution (0.1 M, pH = 7.4) at a constant potential of 0.29 V (Fig. 6a). With each infusion of HY into the electrolyte, a step response emerges rapidly. A rapid increase in oxidation current is related to the early release of HY to the electrode surface. Calibration curve shows peak of the increased current in terms of HY concentration. In Fig. 6b, error bars show standard deviations from amperometric response for the three data analysis rounds. Figure 6c represents two linear slopes, one at concentration range of 2–30 μM [I_P (μA) = $0.0321x + 0.4203$] with LOD of 0.5 and sensitivity of 0.0321 μA μM^{-1} and the other at concentration range of 30 μM–1.5 mM [I_P (μA) = $0.0188x + 0.5743$] with a sensitivity of 0.0188 μA μM^{-1}. Variations in the slope of calibration curves (sensor sensitivity) are due to change in diffusion coefficient of HY, which is smaller as N_2 molecules cover surface of GC electrode. Aggregation of N_2 gas on GC electrode limits diffusion of HY and causes limitation in progress of electrochemical reaction [49]. Given this low LOD, the MSRG/Au nanohybrid is capable of oxidizing HY at low concentrations.

3.2.1 *Intrusive ions, selectivity, stability, and reproducibility*

The MSRG/Au nanohybrid exhibited good reproducibility for oxidation of HY (Fig. 7). The selectivity of the electrode was examined using amperometric response of the GC electrode to 1 mM HY and many interfering ions, as observed after injection of 1 mM HY to PBS (0.1 M) with pH = 7.4. However, no interference effects were detected in amperometric currents by 10-fold and 20-fold injections of nickel nitrate, copper nitrate, uric acid, manganese nitrate, cobalt nitrate, sodium hydroxide, sodium nitrate, iron nitrate, and magnesium chloride. After re-injection of HY, a rapid response to the presence of analyte was given, showing its sensitivity to increasing HY concentration after injection of intrusive ions into the electrolyte, as before.

Reproducibility of the fabricated electrode was also determined by comparing CV of three different

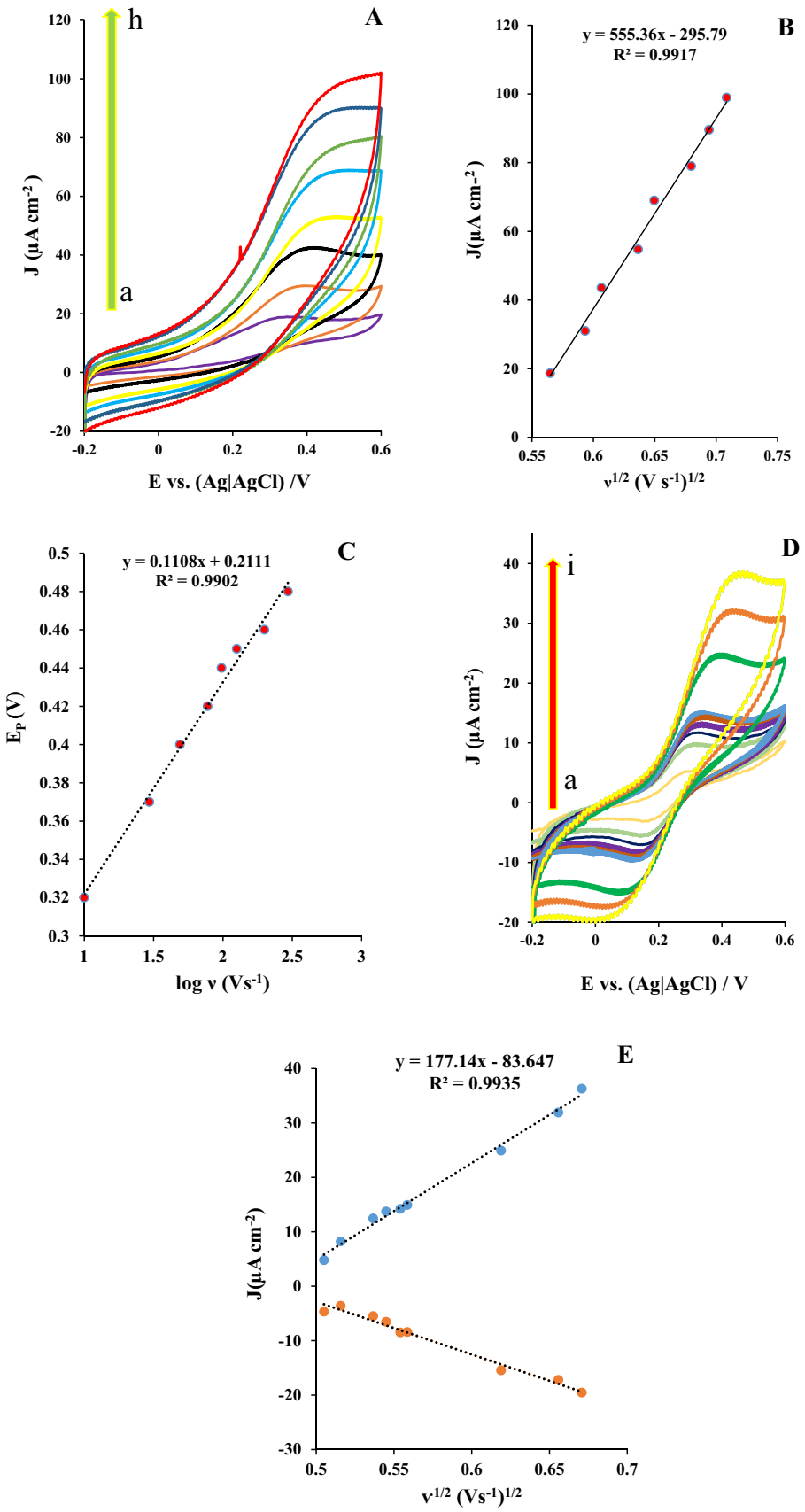

Fig. 5 **a** CVs of MSRG/Au/GC electrode containing 5 mM HY at different scan rates: *a* 10, *b* 30, *c* 50, *d* 70, *e* 90, *f* 100, *g* 200, *h* 300 mVs^{-1}. **b** The plot of I_p vs. $v^{1/2}$, **c** the plot of *Ep* vs. log (*v*), **d** CVs of cvs of MSRG/Au/GE in 1 mM $K_3[Fe(CN)_6]/K_4[Fe(CN)_6]$ containing 0.1 M KCl at scan rates: *a* 10, *b* 30, *c* 50, *d* 70, *e* 90, *f* 100, *g* 200, *h* 300, *i* 400 mVs^{-1}, **e** the plot of I_p vs. $v^{1/2}$

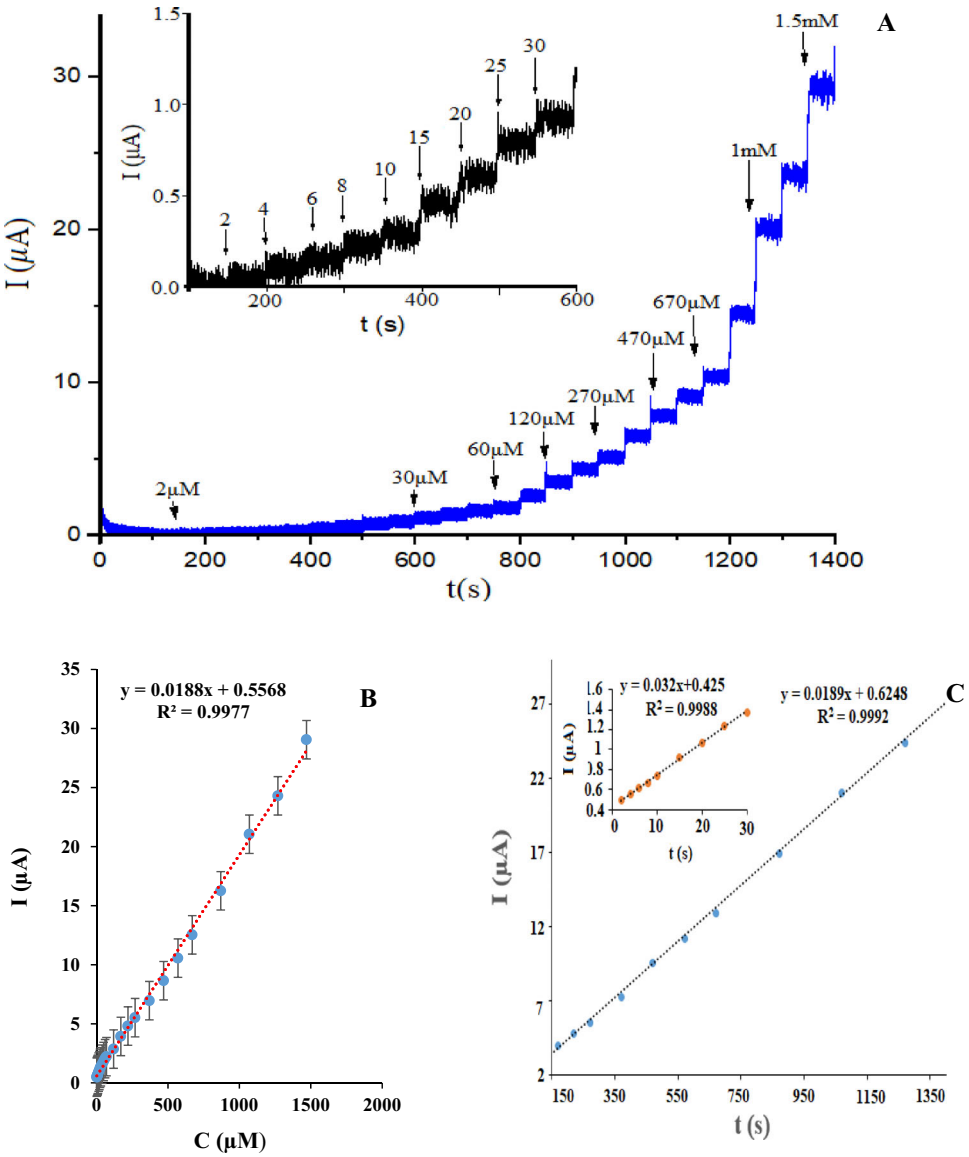

Fig. 6 Amperometric investigation of **a** MSRG/Au/GC electrode by adding HY to stirred solutions at 0.29 V. **b** Error bars show standard deviations from the amperometric response for the three rounds of data analysis. **c** Calibration curves in two ranges of 2–30 and 30–1.5 mM

electrodes at 50 mV s^{-1} in the presence of 1 mM HY. Relative standard deviation (RSD) was equal to 3.7% for these three electrodes. Furthermore, reproducibility of each electrode was performed by eight consecutive CV cycles and an RSD of 4.4% was acquired.

3.3 EIS test

Electrochemical impedance spectroscopy (EIS) measurement is a useful method for investigating electrochemical properties of the materials by changing interfacial properties of the modified electrodes at high frequency. EIS was performed using IRASOL device (IRASOL Co., Iran) in the frequency range between 0.01 and 100 kHz and in open circuit potential in 5 mM K_3 [Fe(CN)$_6$]/K_4 [Fe(CN)$_6$] in 0.1 M KCl solution. All the EIS spectra represented a Nyquist plot with a semicircle at high-frequency region. The semicircle signifies resistance which originates from charge transfer limitation (R_{ct}). In addition, linear response at low frequencies is the evidence regarding the Warburg resistance demonstrating a diffusion-controlled process of electrolyte

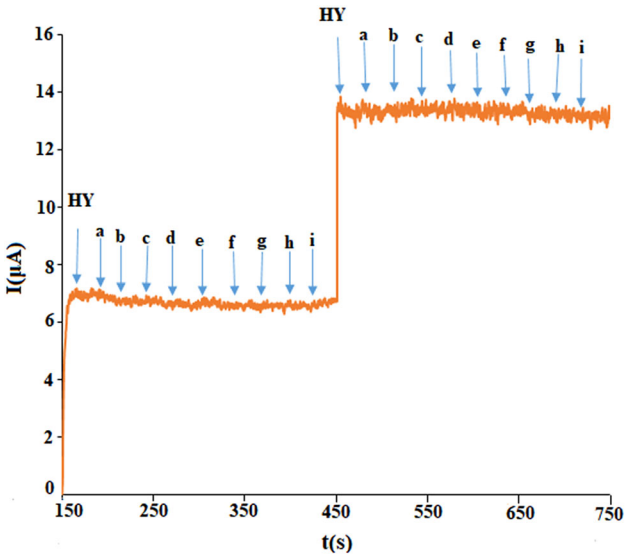

Fig. 7 Amperometric response of MSRG/Au/GC electrode by adding HY to the stirred solutions at a constant potential of 0.29 V in the presence of 10-fold injections and 20-fold injections of *a* nickel nitrate, *b* copper, *c* uric acid, *d* manganese oxide, *e* cobalt nitrate, *f* sodium nitrate, *g* sodium nitrate, *h* iron nitrate, and *i* magnesium chloride

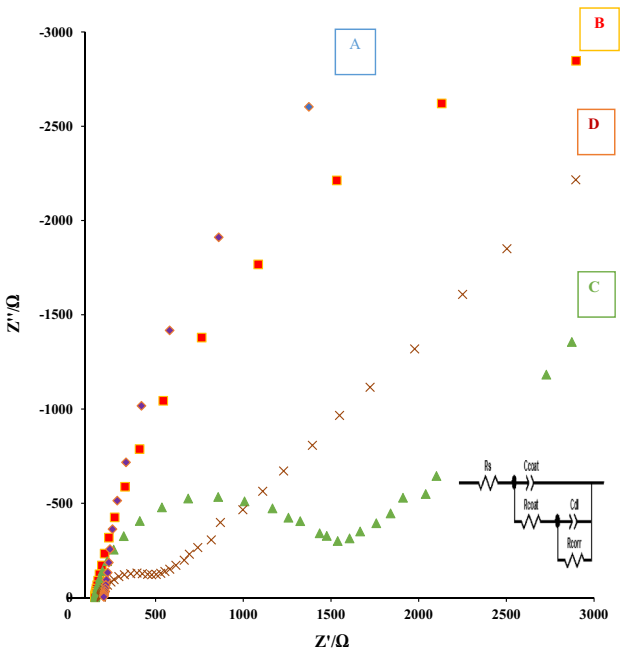

Fig. 8 EIS spectra of *A* bare GC electrode, *B* MoS_2/GC electrode, *C* MSRG/GC electrode, *D* MSRG/Au/GC electrode

ions. Figure 8a–d shows the EIS spectra comparing the GC electrode and the electrode modified with MoS_2, MSRG, and MSRG/Au. The MSRG/Au/GC electrode showed the lowest resistance to charge transfer compared to the MoS_2/GC, MSRG/GC, and unmodified GC electrodes. Charge transfer resistivity of the electrodes modified with the MSRG and MSRG/Au was estimated to be R_{ct} = 500 Ω and R_{ct} = 126 Ω, respectively. The R_{ct} value was estimated to be 25 kΩ and for bare GC electrode was estimated 25 kΩ, which is the largest value among different electrodes. As can be seen, electrocatalytic performance of the MSRG was improved due to the presence of Au in the MSRG/Au nanohybrid.

3.4 Comparison of the performance

Table 1 compares the performance of MSRG/Au/GC electrode for detection of HY with the other electrochemical sensors. The potential at which oxidation of HY occurs, LOD, linear range of concentration, and sensitivity are among the parameters considered in the table. The proposed modified electrode (MSRG/Au/GC) displayed an excellent electrocatalytic activity for the detection of HY with a wide linear range, low LOD, and high sensitivity. High sensitivity and low LOD of the MSRG/Au/GC electrode results from unique porous structure of the nanohybrid and the synergistic effect of the MSRG and Au facilitating transport of electroactive molecules and electrolyte, and electron transfer, respectively.

4 Conclusions

In the present research, a useful MSRG/Au/GC electrode was developed to detect HY with low LOD. The MSRG/Au nanohybrid was synthesized using hydrothermal method and was characterized and performed using some common techniques such as FESEM, EDX, FTIR, TEM, and XRD. Electrochemical activity of the MSRG/Au/GC electrode was analyzed as a function of analyte concentration and amperometric responses. The MSRG/Au/GC electrode showed suitable electrocatalytic behavior toward oxidation of HY with a remarkable decrease in overpotential compared to the MSRG/GC electrode. The synergistic effect of Au with MSRG efficiently improved electrocatalytic activity of the modified electrode. Our results proved that the current-developed MSRG/Au/GC electrode exhibits better or comparable sensing performance in terms of high current density, wide linear range, high sensitivity stability, repeatability, and selectivity for

Table 1 Comparison of different modified electrodes based on MSRG/Au for the detection of HY

Electrode	Linear range	pH	*Ep* (V)	LOD	Sensitivity	References
$CO(OH)_2$ NS-GCE	0.005–3 μM	NaOH	0.45	1.98 μM	2793.9 μA μM^{-1} cm^{-2}	[9]
rGO-Au-CeO_2-GCE	0.01 to 30 μM	PBS	0.35	3 nM	12.40 μA μM^{-1} cm^{-2}	[12]
CNT-NiHCF-GCE	20–200 μM	PBS	0.36	0.8 μM	1217.39 nA μM^{-1} cm^{-2}	[14]
Au-Pd-CB-DHP-GCE	2.5–88 μM	PBS	0.15	1.77 μM	0.0814 μA μM^{-1} cm^{-2}	[15]
Au-Fe_3O_4-GO-GCE	0.0038–1.4 mM	PBS	0.4	0.9 μM	308.1 μA mM^{-1} cm^{-2}	[27]
Au nanocage-rGO-GCE	2–30 μM	PBS	0.17	0.5 μM	0.0377 μA μM^{-1} cm^{-2}	[44]
CuO-OMC-GCE	01–2.11 × 10^3 μM	NaOH	0.4	0.887 μM	0.00487 μA mM^{-1} cm^{-2}	[50]
f-MWCNT-NiHCF-GCE	20–200 μM	PBS	0.35	0.6 μM	1700.14 nA mM^{-1} cm^{-2}	[51]
Fe_3O_4-PPY-GO-GCE	5–1275 μM	PBS	0.15	1.98 μM	31.48 μA μM^{-1} cm^{-2}	[52]
PANI/g-C_3N_4/$AgNP_S$-GCE	5–300 mM	NaOH	0.6	300 μM	–	[53]
Pt/HNPG/GCE	5–6.105 μM	PBS	− 0.1	1.03 μM	3449.68 μA μM^{-1} cm^{-2}	[54]
MSRG/Au-GC	2–30 μM	PBS	0.29	0.5 μM	0.032 μA μM^{-1} cm^{-2}	This work

detection of HY in the presence of interfering ions and species than some reported HY sensors. The MSRG/Au/GC electrode was found to represent the lowest charge transfer resistance compared to bare GC, pure MoS_2/GC, and MSRG/GC electrodes according to the EIS measurements. According to the results, the proposed MSRG/Au nanohybrid may be a promising candidate for the development of electrochemical sensors.

Supplementary Information: The online version contains supplementary material available at https://doi.org/10.1007/s10854-021-05496-3.

References

1. Z. Luo, B. Liu, T. Qin et al., Cyclization of chalcone enables ratiometric fluorescence determination of hydrazine with high selectivity. Sens. Actuators B **263**, 229–236 (2018)
2. S. Manzar, A. Muhammad, N. Baig et al., A new water-stable zinc metal-organic framework as an electrode material for hydrazine sensing. N. J. Chem. **42**, 12486–12491 (2018)
3. K. Mukherjee, T.I. Chio, H. Gu et al., Benzocoumarin hydrazine: a large stokes shift fluorogenic sensor for detecting carbonyls in isolated biomolecules and live cells. ACS Sens. **2**, 128–134 (2017)
4. S. Zhao, L.L. Wang, T.T. Wang et al., Performance hydrazine electrochemical sensor based on gold nanoparticles/single-walled carbon nanohorns composite film. Appl. Surf. Sci. **369**, 36–42 (2016)
5. H. Amin, N.F. Atta, A. Galal, Gold nanoparticles decorated graphene as a high-performance sensor for detection of trace hydrazine levels in the water. Electroanalysis **30**, 1757–1766 (2018)
6. M.M. Shahid, P. Rameshkumar, W.J. Basirunc et al., An electrochemical sensing platform of cobalt oxide @ gold nanocubes interleaved reduced graphene oxide for the selective determination of hydrazine. Electrochim. Acta **259**, 606–616 (2018)
7. Y. Dong, Z. Yang, Q. Sheng, J. Zheng, solvothermal synthesis of Ag@Fe_3O_4 nanosphere and its application as hydrazine sensor. Colloids Surf. A **538**, 371–377 (2018)
8. V.S. Manikandan, Zh. Liu, A. Chen, Simultaneous detection of hydrazine, sulfite, and nitrite based on a nanoporous gold microelectrode. Anal. Chim. Acta **819**, 524–532 (2018)
9. J. Wang, T. Xie, Q. Deng et al., Three-dimensional interconnected $Co(OH)_2$ nanosheets on Ti mesh as a highly sensitive electrochemical sensor for hydrazine detection. N. J. Chem. **43**, 3218–3225 (2019)
10. S. Ghasemi, S. Hosseini, F. Hasanpoor, S. Nabipour, Amperometric hydrazine sensor based on the use of Pt-Pd nanoparticles placed on reduced graphene oxide nanosheets. Microchim. Acta **186**, 601 (2019)
11. M.M. Rahman, V.G. Alfonso, F.F. Santiago, Hydrazine sensors development based on a glassy carbon electrode modified with a nanostructured TiO_2 film by electrochemical approach. Microchim. Acta **184**, 2123–2129 (2017)
12. H. Huang, T. Li, Y. Sun et al., Amperometric Sensing of hydrazine in environmental and biological samples by using CeO_2-encapsulated gold nanoparticles on reduced graphene oxide. Microchip Acta **186**, 46 (2019)
13. A. Kalaivani, S.S. Narayanan, Fabrication of CdSe quantum dots @ nickel hexacyanoferrate core-shell nanoparticles modified electrode for the electrocatalytic oxidation of hydrazine. J. Mater. Sci. **29**, 20146–20155 (2018)

14. N. Vishnu, A.S. Kumar, S. Badhulika, Selective in-situ derivatization of intrinsic nickel to nickel hexacyanoferrate on carbon nanotube and its application for electrochemical sensing of hydrazine. Anal. Chim. Acta **837**, 60–66 (2019)
15. P. Deroco, I. Melo, L. Silva et al., Carbon black supported Au-Pd core-shell nanoparticles within a di hexadecyl phosphate film for the development of hydrazine electrochemical sensor. Sens. Actuators B **256**, 535–542 (2018)
16. F. Asadi, N. Azizi, S. Ghasemi, Preparation of Ag nanoparticles on nano cobalt-based metal-organic framework (ZIF-67) as catalyst support for electrochemical determination of hydrazine. J. Mater. Sci. **30**, 5410–5420 (2019)
17. Z. Meng, M. Li, X. Liu, Z. Lei, Sensitive electrochemical sensor for hydrazine based on in situ synthesis of $Cu_3(BTC)_2$/GO nanocomposite. J. Mater. Sci. **30**, 18617–18625 (2019)
18. G.A. Tig, G. Gunendi, S. Pekyardimic, A selective sensor based on Au nanoparticles-graphene oxide-poly (2,6-pyridine dicarboxylic acid) composite for simultaneous electrochemical determination of ascorbic acid, dopamine, and uric acid. J. Electroanal. Chem. **47**, 607–618 (2017)
19. Sh. Su, X. Han, Z. Lu et al., Facile synthesis of a MoS_2–Prussian blue nanocube nanohybrid-based electrochemical sensing platform for hydrogen peroxide and carcinoembryonic antigen detection. ACS Appl. Mater. Interfaces. **9**, 12773–12781 (2017)
20. M.R. Shahmiri, A. Bahari, H. Karimi-Maleh et al., Ethynylferrocene-NiO/MWCNT nanocomposite modified carbon paste electrode as a novel voltammetric sensor for simultaneous determination of glutathione and acetaminophen. Sens. Actuators B **177**, 70–77 (2013)
21. H. Karimi-Maleh, A. Sanati, V.K. Gupta et al., A voltammetric biosensor based on ionic liquid/NiO nanoparticles modified carbon paste electrode for the determination of nicotinamide adenine (NADH). Sens. Actuators B **204**, 647–654 (2014)
22. R. Sadeghi, H. Karimi-Maleh, A. Bahari, M. Taghvi, A novel biosensor based on ZnO nanoparticles/1, 3-dipropylimida sodium bromide ionic liquid-modified carbon paste electrode for square-wave voltammetric determination of epinephrine. Phys. Chem. Liq. **51**, 704–714 (2013)
23. Y. Shi, Q. Zhang, T. Zhai et al., Localized surface plasmon resonance-enhanced label-free photoelectrochemical immunoassay by Au-MoS_2 nanohybrid. Electrochim. Acta **271**, 361–369 (2018)
24. C. Li, M. Li, X. Bo et al., Facile synthesis of electrospinning Mn_2O_3-Fe_2O_3 loaded carbon fibers for electrocatalysis of hydrogen peroxide reduction and hydrazine oxidation. Electrochim. Acta **211**, 255–264 (2016)
25. S. Ameen, M. Akhtar, H. Shin, Manipulating the structure of polyaniline by exploiting redox chemistry: novel p-NiO/n-polyaniline/n-Si Schottky diode-based chemosensor for the electrochemical detection of hydrazinobenzene. Electrochim. Acta **215**, 200–211 (2016)
26. X. Bo, J. Bai, J. Ju, L. Guo, A sensitive amperometric sensor for hydrazine and hydrogen peroxide-based on palladium nanoparticles onion-like mesoporous carbon vesicle. Anal. Chim. Acta **675**, 29–35 (2010)
27. X. Liu, Z. Yang, Q. Sheng, J. Zheng, one-pot synthesis of Au-Fe_3o_4-Go nanocomposites for enhanced electrochemical sensing of hydrazine. J. Electrochem. Soc. **165**, 596–602 (2018)
28. J. Han, H. Xia, Y. Wu et al., Single-layer MoS_2 nanosheet grafted upconversion nanoparticles for near-infrared fluorescence imaging-guided deep tissue cancer phototherapy. Nanoscale **8**, 7861–7865 (2016)
29. Y. Peng, Zh. Tang, Y.P. Dong et al., Electrochemical detection of hydroquinone based on MoS_2/reduced graphene oxide nanoparticles. J. Electroanal. Chem. **816**, 38–44 (2018)
30. H. Zhang, Ch. Zhai, H. Gao et al., Highly efficient ethylene glycol electrocatalytic oxidation based on bimetallic Pt-Ni on 2D molybdenum disulfide reduced graphene oxide nanosheets. J. Colloid Interface Sci. **547**, 102–110 (2019)
31. K.J. Huang, J.Z. Zhang, Y.J. Liu, L.L. Wang, novel electrochemical sensing plot from based on molybdenum disulfide nanosheets-polyaniline composites and Au nanoparticles. Sens. Actuators B **194**, 303–310 (2014)
32. Y. Li, C.Y. Xu, P.A. Hu, L. Zhen, Carrier central of MoS_2 nanoflakes by functional self-assembled monolayers. ACS Nano **7**, 7795–7804 (2013)
33. S.X. Lee, H.N. Lim, L. Ibrahim et al., Horseradish peroxidase-labeled silver/reduced graphene oxide thin film-modified screen-printed electrode for detection of carcinoembryonic antigen. Biosens. Bioelectron. **89**, 673–680 (2017)
34. G. Vinodha, P.D. Shima, L. Cindrella, Mesoporous magnetite nanoparticles-decorated graphene oxide nanosheets for efficient electrochemical detection of hydrazine. J. Mater. Sci. **54**, 4073–4088 (2019)
35. M. Kakkar, A. Sharma, K.H. Kim, A. Deep, Application of MoS_2 modified screen-printed electrodes for highly sensitive detection of bovine serum albumin. Anal. Chim. Acta **939**, 101–107 (2016)
36. A.S. Dhanjai, B. Tam, Y. Huang et al., MoS_2 nanostructures for electrochemical sensing of multidisciplinary targets. Trends Anal. Chem. **102**, 75–90 (2018)
37. Ch. Zhu, Zh. Zeng, H. Li et al., Single-layer MoS_2-based nanoprobes for homogeneous detection of biomolecules. J. Am. Chem. Soc. **135**, 5998–6001 (2013)
38. F. Luan, Sh. Zhang, D. Chen et al., Cos2-decorated ionic liquid-functionalized graphene as a novel hydrazine electrochemical sensor. Talanta **182**, 529–535 (2018)

39. M.J. Aghagoli, M.H. Beyki, F. Shemirani, Facile synthesis of FeO/MoS nanohybrid for solid-phase extraction of Ag(I) and Pb(II): kinetic, isotherm, and thermodynamic studies. Int. Environ. Anal. Chem. **97**, 1328–1351 (2017)
40. Y.F. Ning, P. Yan, Y.D. Chen et al., Development of a Pt modified microelectrode aimed for the monitoring of ammonium in solution. Environ. Anal. Chem. **97**, 85–98 (2017)
41. L.X. Fang, J.T. Cao, K.J. Huang, A Sensitive electrochemical biosensor for specific DNA Sequence detection based on flower-like Vs_2, graphene and Au nanoparticles signal amplification. J. Electroanal. Chem. **746**, 1–8 (2015)
42. S. Kumar, N.L. Reddy, H.S. Kushwaha, A. Kumar et al., Efficient electron transfer across Zno-MoS-reduced graphene oxide heterojunction for enhanced sunlight-driven photocatalytic hydrogen evolution. ChemSus Chem. **10**, 3588–3603 (2017)
43. O. Akhavan, The effect of heat treatment on formation of graphene thin films from graphene oxide nanosheets. Carbon **48**, 509–519 (2010)
44. S. Daemi, A.A. Ashkaran, A. Bahari, S. Ghasemi, Fabrication of a gold nanocage /graphene nanoscale platform for electrocatalytic detection of hydrazine. Sens. Actuators B **245**, 55–65 (2017)
45. Z. Xiaoli, J. Xu, K. Yan et al., Space-confined growth of MoS_2 and graphene as an active catalyst for hydrogen evaluation reaction. Chem. Mater. **26**, 2344–2353 (2014)
46. H.M.A. Amin, M.F. El-kady, N.F. Atta, A. Galal, Gold nanoparticles decorated graphene as a high-performance sensor for determination of trace hydrazine levels in water. Electro Anal. **30**, 1757–1766 (2018)
47. S. Zhao, L.L. Wang, T.T. Wang et al., A high-performance hydrazine electrochemical sensor based on gold nanoparticles/single-walled carbon nanohorns composite film. Appl. Surf. Sci. **369**, 36–42 (2016)
48. C. Karuppiah, S. Palanisamy, S. Chen et al., A novel and sensitive amperometric hydrazine sensor based on gold nanoparticles decorated graphite nanosheets modified screen-printed carbon electrode. Electrochim. Acta **139**, 157–164 (2014)
49. F. Amiripour, N. Azizi, S. Ghasemi, Gold-Copper bimetallic nanoparticles supported on nano p zeolite modified carbon paste electrode as an efficient electrocatalyst and sensitive sensor for determination of hydrazine. Biosens. Bioelectron. **107**, 111–117 (2018)
50. H. Wu, Sh. Zhou, Y. Wu et al., Ultrafine CuO nanoparticles isolated by ordered mesoporous carbon for catalysis and electroanalysis. J. Mater. Chem. **1**, 14198–14205 (2013)
51. A.S. Kumar, P. Barathi, KCh. Pillai, In situ precipitation of nickel-hexacyanoferrate within multi-walled carbon nanotube, modified electrode and its selective hydrazine electrocatalysis in physiological pH. J. Electroanal. Chem. **654**, 85–95 (2011)
52. Z. Yang, Q. Sheng, S. Zhang et al., One-pot synthesis of Fe_3O_4/polypyrrole/graphene oxide nanocomposites for electrochemical sensing of hydrazine. Microchem. Acta **184**, 2219–2226 (2017)
53. M. Afshari, M. Dinari, M.M. Momeni, The graphitic carbon nitride/ polyaniline/silver nanocomposites as a potential electrocatalyst for hydrazine detection. J. Electroanal. Chem. **833**, 9–16 (2019)
54. Y. Pei, M. Hu, Y. Xia et al., Electrochemical preparation of pt nanoparticles modified nanoporous gold electrode with highly rough surface for efficient determination of hydrazine. Sens. Actuators B **304**, 127416 (2020)

Publisher's Note Springer Nature remains neutral with regard to jurisdictional claims in published maps and institutional affiliations.